Projected Impact of Climate Change on the Energy Budget of the Arctic Ocean by a Global Climate Model

JAMES R. MILLER

Department of Marine and Coastal Sciences, Cook College, Rutgers–The State University of New Jersey, New Brunswick, New Jersey

GARY L. RUSSELL

NASA Goddard, Institute for Space Studies, New York, New York

(Manuscript received 15 October 2001, in final form 20 May 2002)

ABSTRACT

The annual energy budget of the Arctic Ocean is characterized by a net heat loss at the air–sea interface that is balanced by oceanic heat transport into the Arctic. Two 150-yr simulations (1950–2099) of a global climate model are used to examine how this balance might change if atmospheric greenhouse gases (GHGs) increase. One is a control simulation for the present climate with constant 1950 atmospheric composition, and the other is a transient experiment with observed GHGs from 1950 to 1990 and 0.5% annual compounded increases of CO_2 after 1990. For the present climate the model agrees well with observations of radiative fluxes at the top of the atmosphere, atmospheric advective energy transport into the Arctic, and surface air temperature. It also simulates the seasonal cycle and summer increase of cloud cover and the seasonal cycle of sea ice cover. In addition, the changes in high-latitude surface air temperature and sea ice cover in the GHG experiment are consistent with observed changes during the last 40 years.

Relative to the control, the last 50-yr period of the GHG experiment indicates that even though the net annual incident solar radiation at the surface decreases by 4.6 W m^{-2} (because of greater cloud cover and increased cloud optical depth), the absorbed solar radiation increases by 2.8 W m^{-2} (because of less sea ice). Increased cloud cover and warmer air also cause increased downward thermal radiation at the surface so that the net radiation into the ocean increases by 5.0 W m^{-2}. The annual increase in radiation into the ocean, however, is compensated by larger increases in sensible and latent heat fluxes out of the ocean. Although the net energy loss from the ocean surface increases by 0.8 W m^{-2}, this is less than the interannual variability, and the increase may not indicate a long-term trend.

The seasonal cycle of heat fluxes is significantly enhanced. The downward surface heat flux increases in summer (maximum of 19 W m^{-2}, or 23% in June) while the upward heat flux increases in winter (maximum of 16 W m^{-2}, or 28% in November). The increased downward flux in summer is due to a combination of increases in absorbed solar and thermal radiation and smaller losses of sensible and latent heat. The increased heat loss in winter is due to increased sensible and latent heat fluxes, which in turn are due to reduced sea ice cover. On the other hand, the seasonal cycle of surface air temperature is damped, as there is a large increase in winter temperature but little change in summer. The changes that occur in the various quantities exhibit spatial variability, with the changes being generally larger in coastal areas and at the ice margins.

1. Introduction

The Arctic region is one of the key areas in trying to understand how climate might change in the future because it is where the powerful ice–albedo feedback mechanism operates. This feedback leads most global climate models to find enhanced warming in the Northern Hemisphere polar regions in transient studies with increasing atmospheric greenhouse gases (Houghton et al. 1996). Although there are some observational records to identify trends in parts of the Arctic Ocean, satellite datasets are only two decades old, and there is generally not enough long-term information to determine whether the trends are part of natural decadal variability or are the manifestation of climate change. Global climate models have the potential to address this question because they can simulate long-term trends. Serreze et al. (2000) address some of these issues in their summary of studies that document recent change in the northern high-latitude environment.

One of the earliest studies to quantify the various components (both radiative and turbulent) of the Arctic energy budget was that of Fletcher (1965). He used a combination of observations and results from other studies to compile energy budgets for the Arctic Basin at

Corresponding author address: Dr. James R. Miller, Department of Marine and Coastal Sciences, Cook College, Rutgers–The State University of New Jersey, 71 Dudley Road, New Brunswick, NJ 08901.
E-mail: miller@arctic.rutgers.edu

the surface and at the top of the atmosphere (TOA). Nakamura and Oort (1988) used a combination of satellites, rawinsondes, and models to calculate the atmospheric heat budget of both polar regions. Masuda (1990) confirmed their results for the North Polar cap using an independent analysis based on data produced by the European Centre for Medium-Range Weather Forecasts (ECMWF). The availability of polar-orbiting satellites during the last 20 years has helped in compiling better datasets of the Arctic radiative fluxes, both at the surface and at the TOA. However, there are still uncertainties in these fluxes, in part because of the nature of the observations themselves, and in part because of the algorithms used to convert satellite radiances into flux quantities. Chiacchio et al. (2002) and Key et al. (1996) have addressed some of these problems by comparing several different algorithms for the downward longwave flux at the surface in winter. More recently, there have been regional experiments to investigate the various components of the energy budget. One such experiment, the Surface Heat Budget of the Arctic Ocean (SHEBA), was conducted north of Alaska between October 1997 and October 1998 (Andreas et al. 1999; Perovich et al. 1999; Curry et al. 2000; Uttal et al. 2002).

There have been many studies of the Arctic region based on models ranging from one-dimensional column models through three-dimensional coupled atmosphere–ocean models. Tao et al. (1996) found that most of the three-dimensional atmospheric models had a 3°C warm bias in the summer and that most of the models did a poor job of simulating the seasonal cycle of cloud cover. Both sea surface temperature and sea ice cover were prescribed in their study. Another recent intercomparison study by Gates et al. (1999) compared the outputs of 31 different global models to prescribed surface conditions for a 10-yr period. Rinke et al. (2000) compared two different regional climate models with specified ocean temperatures and constrained sea ice for the Arctic and found distinct differences between them, particularly in their moisture budgets. The Arctic is a region of great concern because of the feedbacks that exist and the potential impact of these feedbacks on global climate change. Unfortunately, the complexity of these feedbacks makes the region a difficult one to model, and the remoteness of the region has limited the observations. Randall et al. (1998) provide a good overview of the difficulties of modeling these complex interactions.

The purpose of this paper is to understand how the Arctic energy budget might change in response to increases of atmospheric greenhouse gases and to understand the relationships among the different climate variables that might change. This is accomplished by using two 150-yr simulations from the global climate model of Russell et al. (1995). The first simulation is a control with constant 1950 atmospheric composition, and the second is a greenhouse gas (GHG) experiment with observed greenhouse gas concentrations from 1950 to 1990 and compounded 0.5% annual increases in CO_2 after 1990. These simulations are the same as those used by Miller and Russell (2000) to examine the Arctic freshwater budget. Russell et al. (2000) and Lucarini and Russell (2002) concluded that these model simulations faithfully represent actual climate changes during the past 40 years in the Northern Hemisphere. The climate model is described in the next section. The annual changes in the energy budget are given in section 3, and the seasonal changes in section 4. Section 5 contains a discussion and conclusions. An appendix on model validation provides the reader with some insight on how well the model simulates the present climate.

2. The global climate model

The global synchronously coupled atmosphere–ocean model used in this study was developed by Russell et al. (1995) for climate studies at decade to century timescales. There are 9 vertical layers in the atmosphere and 13 in the ocean. The horizontal resolution for both the atmosphere and ocean is 4° in latitude by 5° in longitude. The resolution for heat, water vapor, and salt is finer than the grid resolution because those quantities have both means and directional gradients inside each grid cell. Atmospheric condensation and ocean vertical mixing are performed on $2° \times 2.5°$ horizontal resolution. The model has several new features including a new ground hydrology scheme, four thermodynamic layers for glacial ice and sea ice, advection of sea ice, glacial ice calving off Antarctica but not in the Northern Hemisphere, and the *k*-profile parameterization (KPP) ocean vertical mixing scheme of Large et al. (1994). Since the model does not use flux adjustments, there is some climate drift. To reduce its effect, predicted model changes are based on the subtraction of the control simulation from the transient GHG experiment.

Unlike rigid-lid ocean models, the present ocean model conserves mass and not volume, has a free surface, and does not use the Boussinesq approximation. The model conserves mass of salt globally at all times and uses natural boundary conditions for precipitation, evaporation, and river flow. The model transports mass, salt, and heat through 12 subresolution straits including the Nares Strait on the west side of Greenland. Continental runoff and glacial ice melting eventually find their way back to the oceans via a river network based on Miller et al. (1994). The area of the Arctic Ocean for this study is 10^7 km^2 and the boundaries (see Fig. 13) are the same as those in Miller and Russell (2000).

The model's clouds are diagnostically determined from the cloud optical depths that are proportional to the square root of the condensate. The global constants of proportionality for each process, moist convection or large-scale condensation, and for each phase, liquid or ice, are chosen to match current radiative observations. When the vertically integrated cloud optical depth is less than 1, then the cloud diagnostics accumulate noth-

TABLE 1. Annual average of Arctic Ocean variables. Ground temperature is an area-weighted composite of ice and ocean surface temperatures. Cloud optical depth is a linear average of cloudy and clear-sky conditions. Numbers in parentheses are twice the std dev of all 150 yr of control data minus their least square fit line. The differences in the last three columns are based on 50-yr averages of the control and GHG simulations.

	Control 1950–2099	GHG experiment minus control		
		1950–99	2000–49	2050–99
Temperature (°C) at 200 mb	−59.89 (0.51)	−0.02	−0.16	−0.02
Temperature (°C) at 500 mb	−35.63 (0.76)	0.27	0.84	1.76
Temperature (°C) at 850 mb	−14.28 (0.98)	0.40	0.99	2.29
Surface air temperature (°C)	−13.08 (1.12)	0.58	1.42	3.41
Ground temperature (°C)	−12.83 (1.22)	0.61	1.49	3.69
Ocean surface temperature (°C)	−1.32 (0.12)	0.06	0.13	0.38
Planetary albedo (%)	56.83 (1.16)	−0.23	−0.76	−1.70
Surface albedo (%)	54.29 (2.67)	−0.76	−2.21	−5.59
Low cloud cover (%)	44.33 (2.57)	0.74	1.57	4.90
Total cloud cover (%)	61.94 (2.81)	1.13	2.69	7.22
Cloud optical depth	6.96 (0.56)	0.23	0.56	1.24
Water vapor (kg m^{-2})	5.67 (0.35)	0.17	0.52	1.11
Ice mass (100 kg m^{-2})	18.35 (1.65)	−0.73	−1.85	−4.23
Sea ice cover (%)	86.54 (3.44)	−1.65	−3.91	−10.81

ing for that time step. When the vertically integrated cloud optical depth is greater than 1, then the cloud diagnostics are accumulated, and the cloud is assumed to be in the layer at which the vertically integrated optical depth from the TOA downward first exceeds 1. Although the model calculates cloud optical depths simultaneously at all levels, the model's cloud diagnostics are constructed so that they are comparable with satellite observations. Low clouds are those that occur between the surface and 740 mb. Low cloud amounts given in Table 1 are a lower bound because only the high cloud is counted when both high and low clouds are present.

Sea ice, which may partially cover any ocean grid cell, has both thermodynamic and dynamic components. The sea ice model uses four thermodynamic layers with a single thickness and rejects all salt when ice is formed. Sea ice velocity is prognostic and is determined by six different terms: atmospheric stress, ocean drag, Coriolis force, gradient of atmospheric pressure and ocean height, internal sea ice pressure gradient, and an island and coastline blocking factor. The omission of parallel side stress may contribute to thinner Arctic sea ice than observed. Sea ice dynamics are described more fully in Miller and Russell (1997). The albedo of sea ice ranges from 0.45 for bare ice to 0.95 for deep fresh snow with values in between for thinner or older snow. Each ocean grid cell has a minimum nonice fraction that is inversely proportional to the ice thickness and that is 6% for 1-m-thick ice. In the Northern Hemisphere in the 150-yr control run, 88% of sea ice is frozen from the ocean and the remainder is created by compacted snow; 78% of sea ice is melted or evaporated from the top and the remainder by encountering warm water. During the melting of sea ice by warm water, the fraction of energy used for vertical melting is equal to the horizontal sea ice cover.

If the net mass crossing an interface by some process is zero, then the net energy transfer by that process can be measured without assuming anything about energy reference levels. If the net mass crossing an interface is not zero, then the energy transfer depends upon the assumed energy reference level, that is, the zero reference temperature and the zero reference phase from which the energy is measured. Hence, radiative transfer and sensible heating can be measured without requiring any assumptions about energy reference levels, but transport and evaporation do require it. The (zero) energy reference level for the atmosphere–ocean model is 0 K for dry air and 0°C for liquid water. Geopotential energy is measured from mean sea level. The energy content of water vapor contains its positive latent heat whereas the energy content of snow or sea ice is negative and is equal to the energy required to warm it to 0°C and melt it to liquid water.

3. Changes in annual energy budget

In this section, changes in the annual energy budget of the Arctic Ocean between the GHG experiment and the control simulation are examined. Since clouds and sea ice have a significant impact on the energy budget, their changes during the 150-yr simulations are discussed first. Figure 1 shows that the total cloud cover over the Arctic Ocean in the control simulation varies between 60% and 65%. Table 1 shows that clouds are increasing in the GHG experiment, with the largest increase during the last 50 years. Numbers in parentheses for a quantity in Table 1 (and subsequent tables) represent twice the interannual standard deviation of the quantity. If a change in the last three columns exceeds the number in parentheses, then the change is significant at the 95% confidence level. Changes in both low clouds and total clouds for the last 50 years of the GHG experiment are statistically significant.

Figure 2 shows that sea ice cover is decreasing in the GHG experiment. Table 1 shows that there is also a

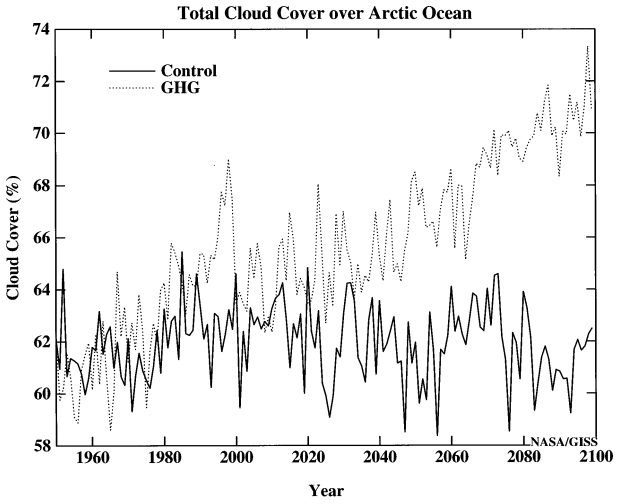

FIG. 1. Mean annual cloud cover over Arctic Ocean for control and GHG simulations.

significant decrease in sea ice mass per unit area in the GHG experiment. The model's sea ice mass can be converted to sea ice thickness by dividing by the product of sea ice density (910 kg m^{-3}) and sea ice cover. For the control the mean annual ice thickness is 2.3 m. Although there is some drift in the model's mean annual sea ice cover for the present climate (from 86% at the beginning to 88% for the control simulation), the drift is much smaller than the decrease in the GHG experiment (10.81%). Mean ice thickness decreases by about half a meter in the GHG experiment. The model's annual export of sea ice from the Arctic Ocean produces an

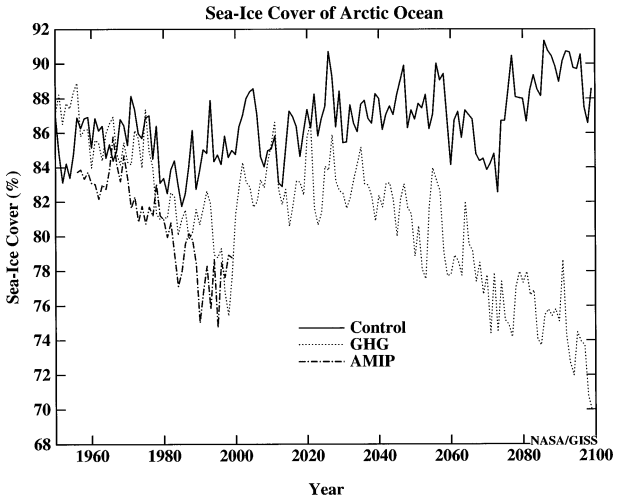

FIG. 2. Sea ice cover of Arctic Ocean for control and GHG simulations and for observations of Atmospheric Model Intercomparison Project (AMIP), which can be downloaded online at http://www-pcmdi.llnl.gov/amip2/AMIP2EXPDSN/BCS/amipobs_dwnld.html. Sea ice cover is defined as the total ice-covered area divided by the domain area. The model and observed values are all for the same area.

TABLE 2. Annual energy budget of the Arctic Ocean (W m^{-2}). Vertical fluxes are positive downward; horizontal transports are positive inward. Numbers in parentheses are twice the standard deviation of all 150 yr of control data minus their least square fit line. The differences in the last three columns are based on 50-yr averages of the control and GHG simulations.

	Control 1950–2099	GHG experiment minus control		
		1950–99	2000–49	2050–99
Radiation (TOA)				
Absorbed solar	79.71 (2.16)	0.43	1.43	3.17
Net thermal	−192.64 (2.03)	−0.19	0.01	−1.44
Net radiation	−112.94 (1.88)	0.24	1.44	1.73
Radiation (atm)				
Absorbed solar	37.12 (0.28)	0.06	0.22	0.42
Net thermal	−163.69 (2.91)	−0.62	−1.08	−3.66
Net radiation	−126.57 (2.78)	−0.55	−0.86	−3.25
Atm heat transport				
Dry	90.26 (3.88)	−0.59	−1.05	−3.33
Latent	12.33 (1.95)	0.30	0.73	0.83
Total	102.59 (4.03)	−0.29	−0.32	−2.51
Radiation (surface)				
Incident solar	92.71 (2.63)	−0.74	−1.87	−4.63
Absorbed solar	42.59 (2.06)	0.37	1.21	2.76
Downward thermal	231.77 (5.65)	2.93	7.09	17.33
Upward thermal	−260.72 (4.91)	−2.50	−6.00	−15.11
Net thermal	−28.96 (1.31)	0.43	1.09	2.22
Surface fluxes				
Net radiation	13.63 (2.20)	0.80	2.30	4.98
Sensible heat	−11.51 (2.10)	−0.40	−0.54	−2.90
Latent heat	−9.79 (1.43)	−0.40	−0.55	−2.61
Precipitation energy	−2.68 (0.20)	−0.05	−0.09	−0.25
Net heat	−10.35 (3.42)	−0.05	1.12	−0.78
Water heat transport				
Rivers	0.07 (0.01)	0.00	0.00	0.00
Sea ice	1.58 (0.86)	−0.02	−0.06	−0.70
Liquid ocean	9.15 (4.16)	0.30	−1.31	0.61
Net energy change	0.44 (3.73)	0.22	−0.25	−0.88

energy import of 1.58 W m^{-2} that decreases by 0.70 W m^{-2} in the GHG experiment (Table 2).

The mean annual components of the energy budget are given in Table 2 with a positive sign denoting a downward vertical flux or an inward horizontal flux into the Arctic. The long-term changes in the radiative fluxes are shown in Fig. 3. Heating rate changes cited in this section are the difference between the last 50 years of the GHG and control simulations. At the TOA, increased clouds cause greater atmospheric reflection that is more than compensated by less surface reflection because of reduced sea ice cover. Thus, Fig. 3a and Tables 1 and 2 show that planetary albedo decreases (from 57% to 55%), and planetary absorption of solar radiation increases by 3.17 W m^{-2}. Increased low clouds, which are often warmer than the surface, cause greater thermal emission to space (Fig. 3b) by 1.44 W m^{-2}, yet the change in net radiation at the TOA in the GHG experiment (Fig. 3c) is still positive downward by 1.73 W m^{-2}.

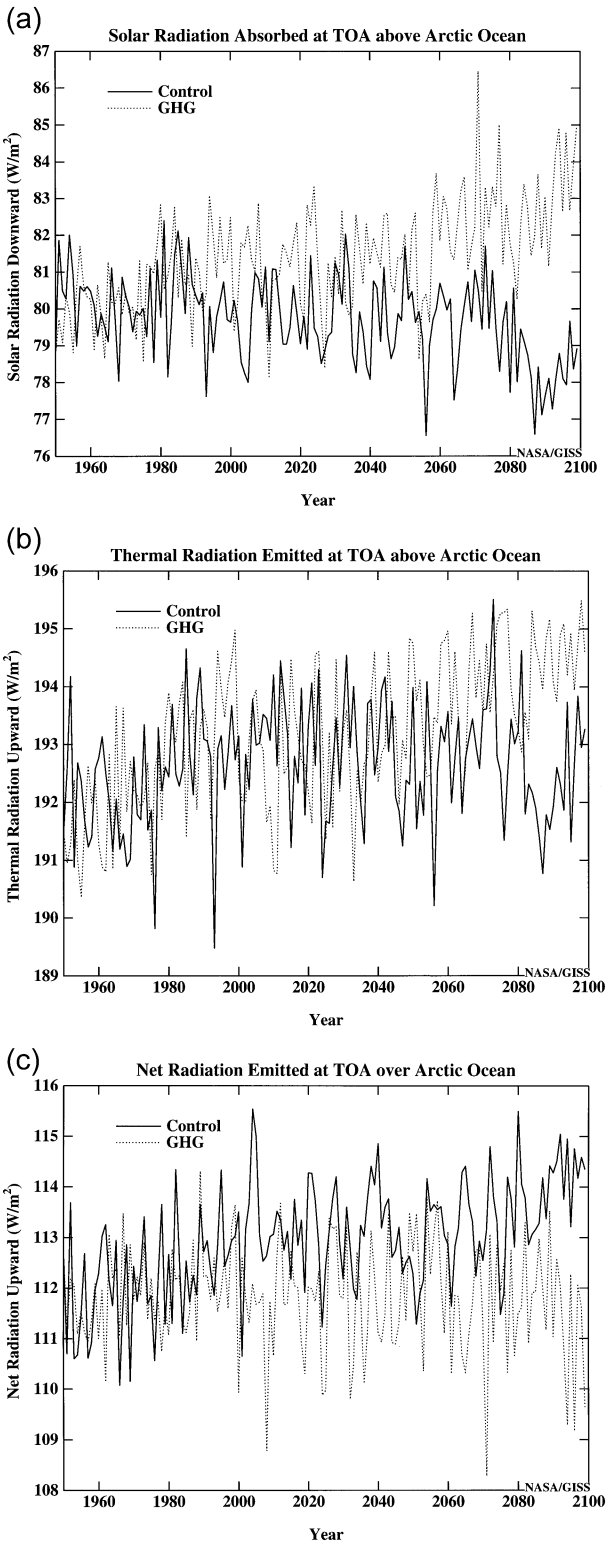

FIG. 3. TOA radiation budget for Arctic Ocean for control and GHG simulations for (a) absorbed solar, (b) outgoing thermal, and (c) net upward radiation.

This is slightly less than the model's global value of 1.8 W m^{-2}.

Within the atmosphere, increased clouds and increased water vapor cause atmospheric absorption of solar radiation to increase by 0.42 W m^{-2} while thermal emission increases by 3.66 W m^{-2}. Increased clouds reduce atmospheric transmission, so that solar radiation incident on the surface (Fig. 4a) decreases by 4.63 W m^{-2}. Nevertheless, Fig. 4b and Table 2 show that solar radiation absorbed by the surface increases by 2.76 W m^{-2} because of decreased sea ice cover. Clouds and increased surface air temperature increase net thermal radiation into the surface (Fig. 4c) by 2.22 W m^{-2} so that the net radiation there (Fig. 4d) increases by 4.98 W m^{-2}. For the control simulation, there is no discernible drift in incident solar radiation at the surface (Fig. 4a), but there are downward drifts in both solar radiation absorbed by the surface (Fig. 4b) and net thermal radiation leaving the surface (Fig. 4c), consistent with the control's increasing sea ice cover. Table 1 shows that the surface albedo decreases from 54% to 49%. For the GHG experiment, greater upward fluxes of sensible heat (2.90 W m^{-2}) and latent heat (2.61 W m^{-2}), and more snowfall (0.25 W m^{-2}) are balanced by greater emission of radiation from the atmosphere (3.25 W m^{-2}) and reduced atmospheric transport of heat into the Arctic air (2.51 W m^{-2}).

Table 2 shows that the changes in each of the components of the surface radiation budget and surface heat flux are statistically significant. Although both Fig. 5 and Table 2 show that the net heat loss from the surface has increased for the last 50 years of the GHG experiment, the opposite occurs in the period from 2000 to 2049, and the change in net surface heat flux is not significant. The change in advective heat loss (0.70 W m^{-2}) due to reduced sea ice export is nearly the same as the gain due to increased liquid heat import (0.61 W m^{-2}). Hence, there is little net change in total oceanic transport of heat into the Arctic Ocean, which is consistent with the small change in surface heat flux. The interannual variability of ocean liquid heat transport is also high, and its change at the end of the GHG experiment is small. Although the decrease in heat export by sea ice is large in comparison to the mean, the variability is also very high.

To summarize the mean annual results, increased cloud cover and decreased sea ice cover in the GHG experiment affect all components of the radiation and surface energy budgets. Greater cloud cover increases atmospheric reflection and absorption and decreases atmospheric transmission of solar radiation. Concurrently, atmospheric thermal emission, both upward and downward, increases. In spite of a decrease of solar radiation incident on the surface, absorption increases owing to reduced sea ice cover. Net thermal radiation also increases into the surface. Reduced sea ice cover causes turbulent fluxes to increase upward. Although the net upward summation of all surface fluxes increases mar-

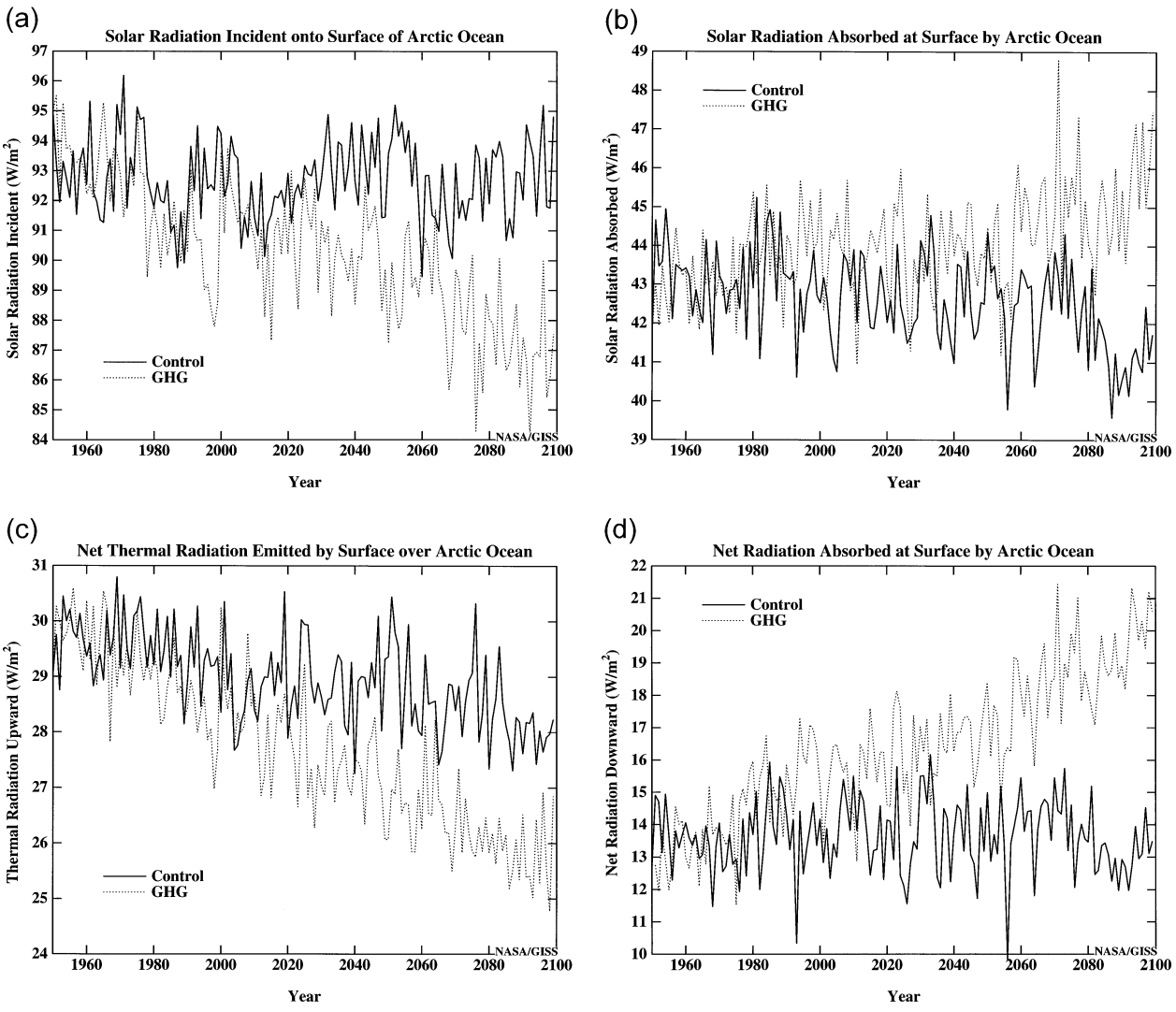

FIG. 4. Surface radiation over Arctic Ocean for control and GHG simulations for (a) incident solar, (b) absorbed solar, (c) net upward thermal, and (d) net downward radiation.

ginally during the last 50 years of the GHG experiment, the change is not statistically significant.

4. Changes in seasonal energy budget

Of perhaps greater interest than changes in the mean annual energy budget discussed in section 3 are seasonal changes in the components of the energy budget. Seasonal changes in polar regions are particularly striking because of the absence of solar radiation during winter. Tables 3 and 4 show the January and July changes for the variables in Table 1. Tables 5 and 6 show the January and July changes for the various components of the energy budget over the Arctic Ocean and can be compared with the annual values in Table 2. The heating rate changes cited in this section are for the last 50 years of the simulations and are shown in the last column of these tables.

As in section 3, changes in clouds and sea ice cover are shown first to better understand how they affect the components of the energy budget. Clouds play a major role in reducing atmospheric transmission for both solar and thermal radiation. Figure 6 and Tables 3 and 4 show that cloud cover increases significantly in winter in the GHG experiment, but there is little change in summer. Cloud optical depth increases in all months, but winter increases are statistically significant and much larger than those in summer. Figure 7 compares the monthly sea ice cover for the control and GHG experiment. Sea ice covers less of the ocean in the GHG experiment during all months with the largest decrease (from 67% to 45%) occurring in September. In January the amount of open water doubles from 5% to 10%.

Changes in seasonal solar fluxes are similar to those in annual solar fluxes taking into consideration that incident solar radiation at the TOA varies from nearly

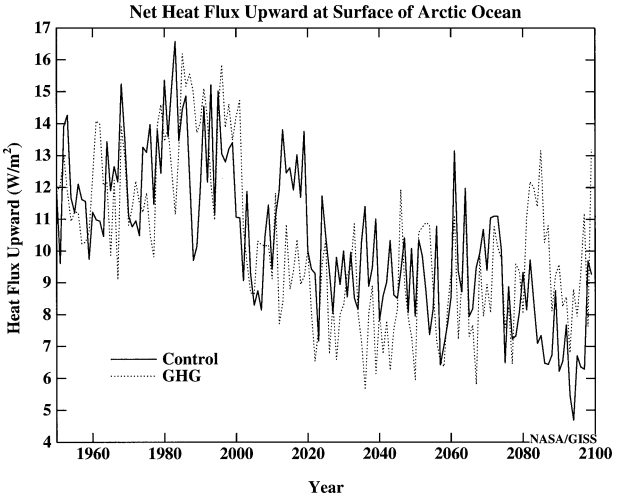

FIG. 5. Net heat flux upward at surface of Arctic Ocean for control and GHG simulations.

zero in December to 505 W m^{-2} in June. Figure 8 and Tables 5 and 6 show that the absorbed solar radiation at the TOA increases in all months in the GHG experiment. At the surface it also increases in all months despite a decrease in incident solar radiation in all months (not shown). Table 6 shows that the July changes in absorbed solar radiation at the TOA and at the surface are almost significant but that the changes in incident radiation at the surface are smaller than natural variability. The decrease in sea ice cover, with greatest reduction in summer, enhances both the annual magnitude and seasonal cycle of solar absorption. Cloud changes, which are smaller in summer, attempt to reduce solar absorption but are overwhelmed by the sea ice changes.

Changes in seasonal thermal fluxes are shown in Fig. 9. In winter, the cloud layer is warmer than both the surface and the upper atmosphere. Because there are more clouds, atmospheric thermal emission increases (6.42 W m^{-2}) sending its radiation both upward and downward. Outgoing thermal radiation at the TOA increases by 3.17 W m^{-2}. Upward thermal radiation at the surface increases for two reasons in winter: there is more open water whose ocean temperature is considerably warmer than that of sea ice and the surface temperature of sea ice is warmer in the GHG experiment. Nevertheless, downward thermal radiation still dominates at the surface and the net upward emission decreases by 3.24 W m^{-2}. In summer, the temperature contrast between ocean and ice disappears and the surface is warmer than the cloud layer. The small increase in cloud optical thickness further insulates the warm surface from outer space while hardly changing the net atmospheric thermal emission. Upward thermal radiation decreases by 0.97 W m^{-2} at the TOA and by 0.88 W m^{-2} at the surface in summer.

The changes in atmospheric energy transport into the Arctic in the GHG experiment are different between winter and summer (Tables 5 and 6). The transport is reduced in winter, in part because the higher polar surface air temperature weakens the latitudinal temperature gradient. The transport is higher in summer. Although atmospheric transports into the Arctic respond to changes in other processes, it is also likely that they participate in driving some of the Arctic changes.

Figure 10 shows the net heating at the surface. During winter, the net heat loss out of the Arctic Ocean increases by 10–16 W m^{-2}, and during summer the flux into the ocean increases by almost 20 W m^{-2} in June. As noted in section 3 (Fig. 5 and Table 2), the variability in mean annual net heating of the ocean surface between the three different 50-yr periods of the GHG experiment makes it difficult to determine whether there is a long-term trend. This is in contrast to the unambiguous seasonal changes in net surface heating where the seasonal cycle is significantly enhanced. The reduction of upward surface heat flux by radiation in January (Table 5) is overwhelmed by increases of the other components (8.4 W m^{-2} by sensible heat, 5.16 W m^{-2} by latent heat, and 0.67 W m^{-2} by precipitation heat). The turbulent fluxes in winter are proportional to the open water fraction; both the fluxes and open water nearly double in January. In July (Table 6), the warmer, moister Arctic

TABLE 3. Arctic Ocean variables for Jan (otherwise like Table 1).

	Control	GHG experiment minus control		
	1950–2099	1950–99	2000–49	2050–99
Temperature (°C) at 200 mb	−61.35 (2.37)	−0.14	−0.67	−0.60
Temperature (°C) at 500 mb	−42.33 (2.75)	0.30	0.33	1.16
Temperature (°C) at 850 mb	−24.04 (3.35)	0.58	0.71	2.46
Surface air temperature (°C)	−25.97 (3.32)	0.76	1.70	5.11
Ground temperature (°C)	−26.11 (3.58)	0.85	1.89	5.81
Ocean surface temperature (°C)	−1.66 (0.07)	0.01	0.01	0.12
Low cloud cover (%)	23.85 (8.78)	1.11	2.05	11.46
Total cloud cover (%)	31.22 (9.92)	1.99	2.66	13.65
Cloud optical depth	2.46 (1.08)	0.34	0.31	1.25
Water vapor (kg m^{-2})	1.99 (0.57)	0.13	0.12	0.53
Ice mass (100 kg m^{-2})	18.10 (1.91)	−0.63	−2.14	−4.84
Sea ice cover (%)	94.14 (2.23)	−0.84	−0.60	−4.91

TABLE 4. Arctic Ocean variables for Jul (otherwise like Table 1).

	Control 1950–2099	GHG experiment minus control		
		1950–99	2000–49	2050–99
Temperature (°C) at 200 mb	−56.68 (0.94)	0.18	0.06	0.43
Temperature (°C) at 500 mb	−25.09 (1.45)	0.46	1.26	2.07
Temperature (°C) at 850 mb	−1.43 (1.31)	0.31	0.93	1.63
Surface air temperature (°C)	0.21 (0.30)	0.14	0.26	0.60
Ground temperature (°C)	0.00 (0.16)	0.09	0.14	0.46
Ocean surface temperature (°C)	−0.80 (0.23)	0.11	0.24	0.69
Planetary albedo (%)	52.39 (1.89)	−0.13	−0.68	−1.84
Surface albedo (%)	40.06 (1.79)	−0.76	−1.81	−5.07
Low cloud cover (%)	58.35 (4.40)	−0.94	−0.45	−0.82
Total cloud cover (%)	85.33 (3.37)	−0.02	−0.19	−0.64
Cloud optical depth	12.25 (2.59)	0.26	0.32	0.08
Water vapor (kg m^{-2})	12.52 (1.16)	0.42	1.04	1.79
Ice mass (100 kg m^{-2})	15.68 (2.41)	−1.00	−2.58	−5.72
Sea ice cover (%)	84.86 (4.78)	−2.07	−5.01	−14.00

air reduces the effectiveness of the turbulent fluxes, and their small changes are now additive to the increased solar absorption.

Figure 11 shows that the ocean liquid heat transport into the Arctic Ocean increases in all months in the GHG experiment with the largest increases occurring in July, November, and December. However, there is no significant change in total ocean heat transport because the increase by liquid transport is opposed by a decrease in sea ice transport of energy. Table 2 shows that the changes are nearly offsetting. The other component of the water transport is due to river flow, which is always small.

TABLE 5. Jan energy budget (W m^{-2}) of the Arctic Ocean (otherwise like Table 2).

	Control 1950–2099	GHG experiment minus control		
		1950–99	2000–49	2050–99
Radiation (TOA)				
Absorbed solar	0.11 (0.01)	0.00	0.00	0.00
Net thermal	−169.28 (6.86)	−0.52	−0.50	−3.18
Net radiation	−169.17 (6.85)	−0.52	−0.50	−3.17
Radiation (atm)				
Absorbed solar	0.08 (0.00)	0.00	0.00	0.00
Net thermal	−129.92 (11.35)	−1.17	−1.03	−6.42
Net radiation	−129.84 (11.35)	−1.17	−1.02	−6.42
Atm heat transport				
Dry	105.92 (14.27)	−1.09	−1.86	−7.73
Latent	7.46 (4.06)	0.59	−0.06	−0.08
Total	113.38 (14.47)	−0.51	−1.92	−7.81
Radiation (surface)				
Incident solar	0.10 (0.02)	0.00	0.00	−0.01
Absorbed solar	0.03 (0.01)	0.00	0.00	0.00
Downward thermal	172.72 (16.58)	3.73	7.41	24.00
Upward thermal	−212.08 (12.16)	−3.09	−6.89	−20.75
Net thermal	−39.36 (5.13)	0.64	0.52	3.24
Surface fluxes				
Net radiation	−39.33 (5.13)	0.64	0.52	3.25
Sensible heat	−9.40 (5.05)	−0.89	−1.91	−8.40
Latent heat	−5.35 (2.61)	−0.63	−0.91	−5.16
Precipitation energy	−1.71 (0.55)	−0.16	−0.11	−0.67
Net heat	−55.79 (10.09)	−1.03	−2.42	−10.99
Water heat transport				
Rivers	−0.01 (0.00)	0.00	0.00	0.00
Sea ice	2.14 (1.74)	0.17	0.28	−0.50
Liquid ocean	7.40 (4.91)	0.39	−1.44	0.26
Net energy change	−46.26 (9.20)	−0.48	−3.58	−11.23

Changes in surface air temperature are closely related to changes in the energy budget. Table 1 shows that the mean annual surface air temperature increases by 3.41°C during the last 50-yr period of the GHG experiment, and Fig. 12 shows that it increases in all months. It does not, however, increase uniformly in all months. The increases are up to 6°C in winter, smaller in spring and autumn, and quite small in summer. Changes in surface air temperature are driven by increased upward turbulent fluxes in winter and by increased atmospheric transport in summer. The increased amplitude of the annual cycle of net surface heating is consistent with the reduced amplitude for surface air temperature. The increased heat flux from the ocean in winter increases the surface air temperature significantly, while the increased heat flux into the ocean in summer has little effect on the summer air temperature.

The results to this point are for the entire Arctic Ocean. Figure 13 shows the spatial variability of the January and July changes in three variables: surface air temperature, sea ice cover, and surface heat flux. A general feature of the panels is that the changes tend to be larger near the coasts and are most pronounced in the Barents Sea, which is located in the center of the upper-right quadrant of the figures. For surface air temperature, the changes are small almost everywhere in summer and increase significantly in winter, with the greatest increases in the Barents Sea and off the coast of Alaska. In July, the change in the surface heat flux into the ocean is largest along the coast with a secondary maximum near the North Pole.

The seasonal results can be summarized as follows. Cloud cover (except in summer) and cloud optical depth

TABLE 6. Jul energy budget (W m^{-2}) of the Arctic Ocean (otherwise like Table 2).

	Control 1950–2099	GHG experiment minus control 1950–99	2000–49	2050–99
Radiation (TOA)				
Absorbed solar	220.49 (8.72)	0.50	3.19	8.64
Net thermal	−221.10 (2.68)	0.55	0.90	0.97
Net radiation	−0.61 (6.66)	1.05	4.09	9.61
Radiation (atm)				
Absorbed solar	93.23 (1.09)	0.18	0.51	0.72
Net thermal	−204.99 (3.21)	0.06	0.03	0.09
Net radiation	−111.77 (2.38)	0.24	0.54	0.81
Atm heat transport				
Dry	75.00 (8.27)	0.73	1.96	3.81
Latent	21.15 (8.16)	0.62	1.28	1.01
Total	96.16 (6.37)	1.35	3.24	4.81
Radiation (surface)				
Incident solar	211.82 (12.42)	−2.18	−2.11	−3.96
Absorbed solar	127.26 (8.52)	0.32	2.68	7.92
Downward thermal	299.60 (3.34)	0.93	1.52	3.08
Upward thermal	−315.70 (0.77)	−0.44	−0.65	−2.20
Net thermal	−16.11 (3.26)	0.49	0.87	0.88
Surface fluxes				
Net radiation	111.15 (6.17)	0.81	3.55	8.80
Sensible heat	−4.39 (2.37)	0.81	1.59	2.36
Latent heat	−8.18 (2.64)	0.69	1.97	2.65
Precipitation energy	−3.04 (0.77)	0.10	0.22	0.62
Net heat	95.54 (7.78)	2.40	7.33	14.43
Water heat transport				
Rivers	0.14 (0.03)	0.00	0.01	0.02
Sea ice	0.66 (1.29)	0.03	0.01	−0.49
Liquid ocean	7.83 (4.77)	−0.01	−1.45	0.36
Net energy change	104.17 (9.01)	2.42	5.90	14.31

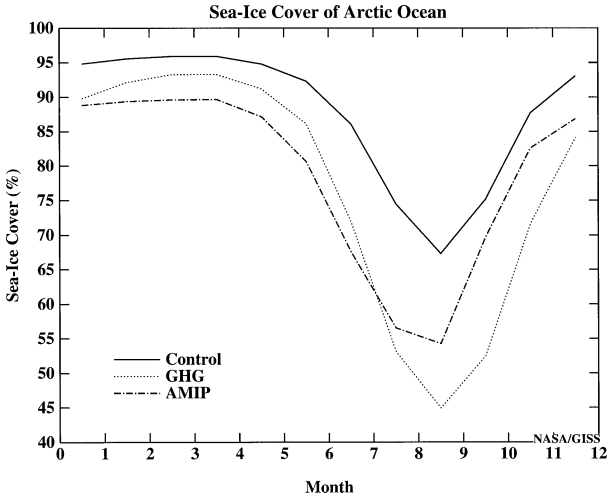

FIG. 7. Monthly sea ice cover for control and GHG simulations and for AMIP observations (see Fig. 2 caption).

increase while sea ice cover decreases in all seasons. The reduced sea ice cover causes absorbed solar radiation into the ocean to increase in summer and upward turbulent fluxes to increase in winter, both of which enhance the seasonal cycle of surface energy fluxes. The increased winter cloud cover increases the thermal radiative loss to space, thus enhancing the TOA radiative seasonal cycle. The increased winter cloud cover also increases the downward thermal radiation at the surface, partially offsetting the large increase in upward turbulent fluxes. In summer, a small decrease in low clouds and increase in higher clouds reduces net upward thermal radiation whose small change is now additive to the increased solar radiation that dominates. The warmer, moister surface air also reduces the upward turbulent

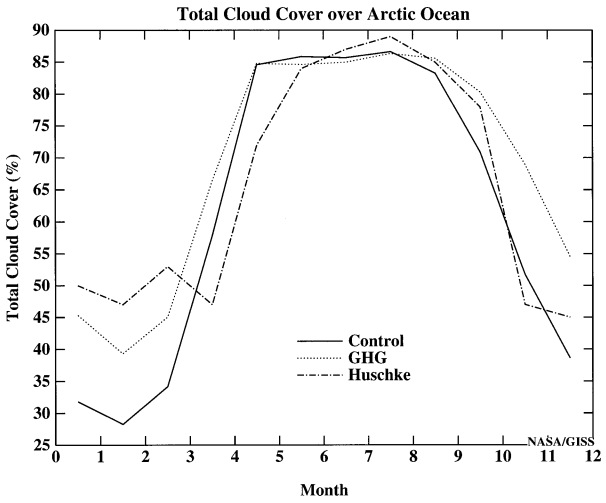

FIG. 6. Monthly cloud cover over Arctic Ocean for control and GHG simulations, and for observations of Huschke (1969).

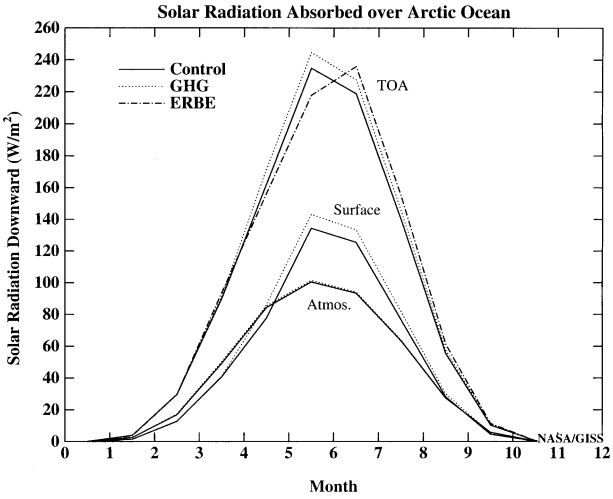

FIG. 8. Monthly solar radiation absorbed over Arctic Ocean for control and GHG simulations at the TOA, by the atmosphere, and at the surface. Observed solar radiation at the TOA from the Earth Radiation Budget Experiment (ERBE; Barkstrom et al. 1989).

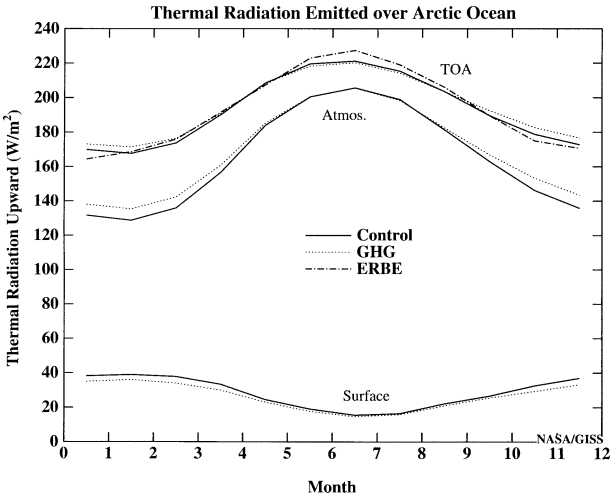

FIG. 9. Monthly net thermal radiation upward over Arctic Ocean for control and GHG simulations at the TOA, from the atmosphere, and from the surface. Observed thermal radiation at the TOA is from ERBE.

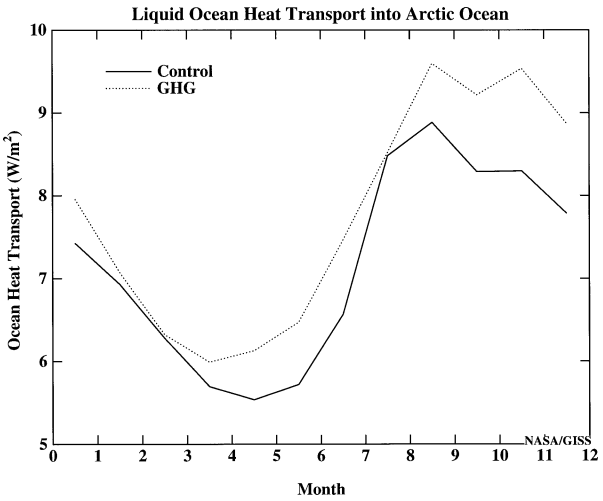

FIG. 11. Monthly liquid ocean heat transport into Arctic Ocean for control and GHG simulations.

fluxes. Thus, the changes in each term of the TOA and surface fluxes enhance the seasonal cycle in summer. For surface air temperature the seasonal cycle is damped, and the January increase (5.11°C) is an order of magnitude larger than the summer increase (0.60°C).

5. Discussion and conclusions

The simulations in this paper are the same as those used to examine potential changes in the Arctic freshwater and mass budgets (Miller and Russell 2000). In the GHG experiment there are net increases of river flow, precipitation, and evaporation and net decreases of sea ice cover and sea ice export from the Arctic Ocean. The net reduction in total oceanic heat flux into the Arctic Ocean is small (and statistically insignificant) because the decrease owing to reduced sea ice export is nearly cancelled by the increased liquid heat transport.

The mean annual results and seasonal results are summarized in the last paragraphs of sections 3 and 4. Changes in the mean annual components of the energy budget and related variables are the sum of seasonal changes that are often quite different, and in some cases, of opposite sign. The amplitudes of the seasonal cycles of the following variables increase in the GHG experiment: sea ice cover, solar radiation absorbed at TOA and surface, net radiation at TOA, turbulent heat fluxes, and net heating at the surface. Variables whose amplitudes decrease include cloud cover, atmospheric poleward heat transport, and surface-air temperature. When the mean annual change is the difference between large seasonal changes of the same magnitude, but opposite

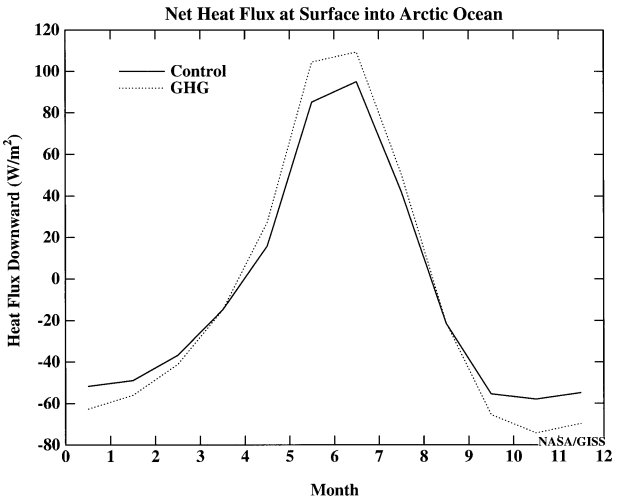

FIG. 10. Monthly net heat flux at surface into Arctic Ocean for control and GHG simulations.

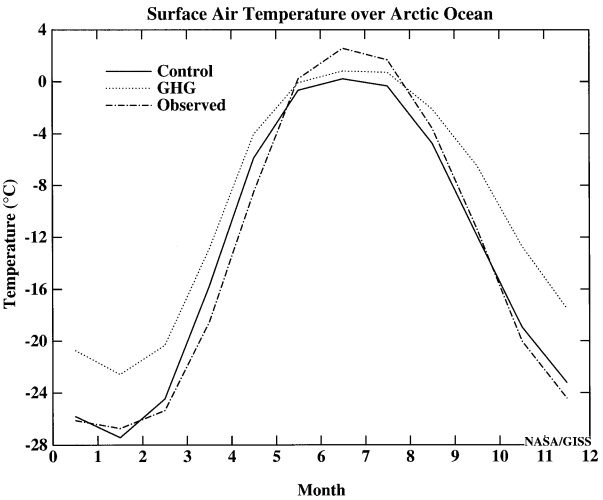

FIG. 12. Monthly surface air temperature for control and GHG simulations and for the observations of Shea (1986).

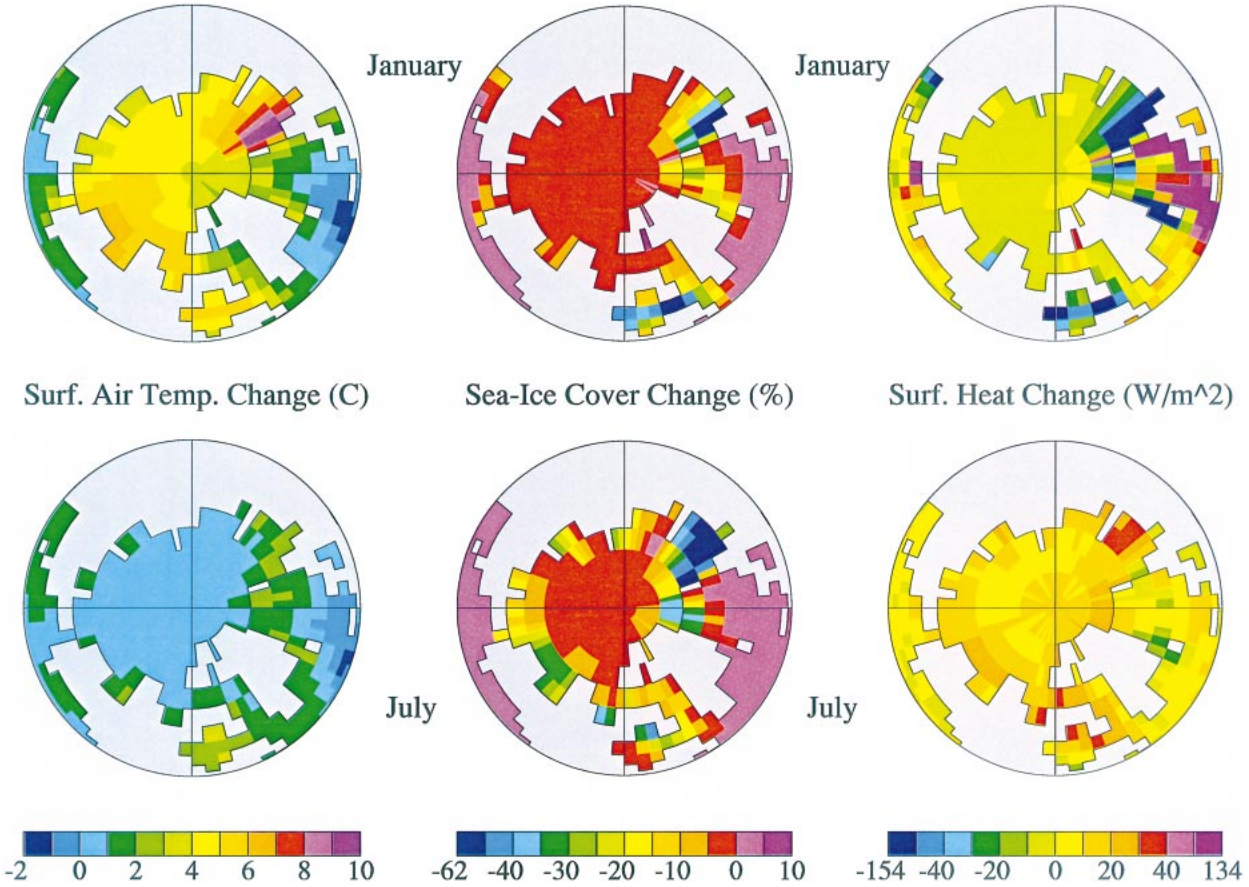

FIG. 13. Changes in (left) surface air temperature, (center) sea ice cover, and (right) net surface heat flux for (top) Jan and (bottom) Jul for the last 50 years of the GHG experiment minus the control simulation. The boundaries of the Arctic Ocean for this study are shown as thin black lines across the Bering Strait, between Greenland and Spitzbergen, between Spitzbergen and Norway, and by the 90° meridian through the McClure Strait. The prime meridian is toward the right.

sign, it may be difficult to determine the mean annual change. An example of this is the net heating at the surface for which there is a significant increase of heat into the ocean in summer and out of the ocean in winter. The GHG experiment does not allow one to conclusively determine whether there is a net change or trend in the mean annual surface heating. The winter change is smaller than the summer change, but it extends over more months.

Changes in the energy budget and surface air temperature are closely related. Serreze et al. (2000) indicate that most climate models find the greatest Arctic warming in autumn and winter, but observations show greater warming from winter to early summer, presumably because of increased atmospheric heat flux into the region. The atmospheric heat transport into the Arctic does increase in summer in the GHG experiment, but it does not cause much change in the surface air temperature, which is constrained by the presence of sea ice and ocean surface temperatures that cannot increase much above the freezing point. The large increase in surface air temperature in winter is primarily due to local processes. In fact, the model's decreased atmospheric heat transport into the Arctic in winter tends to reduce the warming. Serreze et al. (2000) are careful to point out that changes in the Arctic are still difficult to observe for many reasons. There are few data in many regions; the changes that have occurred during the last 40 years occur in part because of changes in the North Atlantic Oscillation (NAO); and some of the data are difficult to interpret. Changes in surface air temperature in the GHG experiment are discussed in greater detail in Russell et al. (2000) and in Lucarini and Russell (2002). They showed that the model's surface air temperature and pressure changes during the last 40 years are well correlated with observed changes in the Northern Hemisphere winter.

There are few global coupled atmosphere–ocean–ice models that have specifically examined the energy budget of the Arctic. One such study is that of Weatherly and Zhang (2001) who used a global model with a much higher resolution ocean model (0.67° in latitude and longitude) than the one used in the present study. Our results for the last 50 years of the GHG experiment

correspond roughly to their doubled CO_2 results. For both models the control sea ice thickness is between 2 and 3 m, and both thin by about 0.5 m in the GHG experiment. For both models the control sea ice extent is larger than observed with too much in coastal areas, and both models show a decrease of about 10% in sea ice cover in the GHG experiment. Both models show decreased incident solar radiation at the surface, increased downward thermal radiation, and increased cloud cover. Both models show enhanced warming of surface air temperature in winter, 6.2° in theirs and 5.1°C in ours. These are lower increases than some other models, possibly because the sea ice extent is too large in both.

There are many complex interactions among radiation, clouds, and surface fluxes in the Arctic Ocean. Although some of these interactions have been discussed in this paper, there are many others that are considered in a comprehensive treatment by Fletcher (1965). He notes that solar radiation reflected upward from the surface in summer is reflected back downward by clouds; the diffuse component of solar radiation is often significantly higher than the direct component; and the melt of snow and ice and the subsequent puddling of liquid water on sea ice can significantly alter the surface albedo in summer. The model used here does account for multiple scattering of sunlight by clouds and does distinguish between direct and diffuse radiation, but we have not quantified these effects. Although the model does not include puddling explicitly, the model's sea ice albedo does decrease to 45% after the snow has melted, which implies that the effects of puddling on albedo are included implicitly.

It is difficult to sort out all the related feedbacks that interact to produce the changes in the components of the energy budgets in the GHG experiment. For sea ice alone there are seasonally varying changes in albedo, thickness, and geographic coverage. For clouds there are seasonally varying changes in total cloud cover, high and low clouds, and optical depth. In addition, there is an increase in atmospheric water vapor with the largest increase occurring in summer. Changes in these variables affect the surface radiative and turbulent fluxes. One example of the competing interactions between sea ice and clouds is the increase in absorbed solar radiation at the TOA and the surface in the GHG experiment. At the TOA the absorbed solar radiation increases in spite of the increased reflectivity of the atmosphere (more clouds). At the surface, reduced sea ice cover accounts for the absorbed solar radiation increasing in spite of a decrease in incident solar radiation.

One of the strongest high-latitude feedbacks is thought to be the ice–albedo feedback mechanism in which a positive temperature perturbation will melt sea ice, thus lowering the surface albedo and increasing the absorbed solar radiation that causes the temperature to increase even more. This feedback mechanism is operative in the GHG experiment in summer. In July the surface albedo has decreased from 40% in the control to 35% at the end of the GHG experiment. The sea ice cover is 14% lower, the absorbed solar radiation has increased by 7.92 W m^{-2}, and the ocean surface temperature and surface air temperature have increased by 0.69° and 0.60°C, respectively. However, not all of the increased surface air temperature in July can be attributed to this feedback. Table 6 shows that the atmospheric heat transport into the Arctic has increased while the upward turbulent fluxes decreased, which means that changes in atmospheric dynamics are the driving contribution to the increased air temperature in summer.

In winter, the ice–albedo feedback mechanism described above is inoperative because the solar radiation is negligible. The gradually increasing summer meltback, however, means there is more open water in the fall and more heat and water vapor can be released into the atmosphere. This introduces a positive cloud feedback as clouds increase by 13.65% in January and contribute to a 24.00 W m^{-2} increase in downward thermal radiation thus heating the sea ice and open water surfaces. Table 5 shows that the change in net radiation at the surface (3.25 W m^{-2}) is small in comparison to the large increases in turbulent fluxes that occur primarily because there is 5% more open water in January in the GHG experiment. Deser et al. (2000) used reanalysis products to examine relationships between sea ice variability, sea level pressure, and surface air temperature. They found that the positive ice–albedo feedback mechanism may contribute to summer ice retreat, a result consistent with the results of the present study. They also found support for the hypothesis that anomalous sea ice concentration is forced by changes in atmospheric circulation. Although the effect of changes in atmospheric circulation on sea ice variability are important in the model, the changes in January and July atmospheric heat transport into the Arctic are not statistically significant, and on an annual average, atmospheric heat transport into the Arctic decreases in the GHG experiment. Changes in atmospheric stress, which can affect sea ice advection, have not been examined.

Rind et al. (1995, 1997) used a very different model to determine how the sea ice–albedo feedback mechanism interacts with other feedbacks, particularly those related to clouds and water vapor. They found that the total effect of sea ice, including feedbacks, accounted for about one-third of the global change in surface air temperature in a doubled CO_2 simulation. They also found that the effect was 4 times larger than an analysis that left out cloud and water vapor feedbacks that resulted from changes in sea ice cover. The GHG results here are consistent with their results in winter when the largest increase in surface air temperature occurs, in part, because increased clouds and water vapor enhance the surface warming in winter.

One strength of the model used here is that it simulates the annual cycle of cloud cover well. This occurs, in part, because the model's atmospheric energy trans-

port into the region, including latent energy, is consistent with observations. The combination of atmospheric transport of water and surface evaporation provides sufficient atmospheric water to condense into clouds. One weakness of the model for the present study is that the model's sea ice cover is too high in both summer and winter, particularly near the coasts. This discrepancy between the model and observations limits the model's predictive capability. On the other hand, the internal self-consistency of the model and the ability to compare the results here with the changes in the hydrologic cycle discussed in Miller and Russell (2000) help to frame some of the questions related to potential climate change in the Arctic region. In spite of the many difficulties in both observing and modeling the Arctic region, it is hoped that other climate modelers will focus on potential changes in the Arctic energy budget to determine whether their results are similar to or significantly different from those presented here.

Acknowledgments. Partial support for JRM has been provided by NASA Grant NAG5-11720 and by Project #32103 of the New Jersey Agricultural Experiment Station. We are grateful to Jennifer Francis and Bill Lipscomb for reviewing the manuscript and providing many helpful suggestions to improve it. We would also like to thank John Weatherly and Yonghua Chen for helpful discussions and constructive comments. Additional information about these simulations is available online at http://aom.giss.nasa.gov.

APPENDIX

Validation of Control Simulation for Present Climate

Reliable observations of most geophysical quantities in the Arctic are lacking so model validation is difficult. In this section we provide information about the model's control simulation to provide some indication of how well the model represents the various components of the energy budget. Of all the components of the Arctic energy budget, those for which we have the most reliable observations are the TOA radiative fluxes. Figures 8 and 9 show that the model is in generally good agreement with the satellite observations from the Earth Radiation Budget Experiment (ERBE; Barkstrom et al. 1989). Our results can be compared with those of Nakamura and Oort (1988) who use a combination of satellites, rawinsondes, and models to compile an Arctic energy budget, and with the analysis of Masuda (1990). The comparison is not exact because our study is for the Arctic Ocean and theirs was for the latitude band between 70° and 90°N. The absorbed solar radiation at the TOA in our study is maximum in summer at 235 W m^{-2} compared to Nakamura and Oort's 210 W m^{-2}.

Based on Table 2 the control simulation's net annual radiation into the Arctic Ocean is 13.6 W m^{-2}. The results for the net annual radiative fluxes at the surface are within 10 W m^{-2} of the observations of Nakamura and Oort (1988). The surface radiative fluxes are difficult to observe, particularly thermal radiation. Beesley (2000) indicates that there can be model errors of 10 W m^{-2} in the downward thermal radiation in winter when low clouds are present. Chiacchio et al. (2002) and Key et al. (1996) compare several different methods for retrieving downward thermal fluxes in winter and find biases ranging from -34 W m^{-2} to nearly zero. Chiacchio et al. (2002) conclude that the possible sources of errors include clouds that are too thin, lack of cloud overlap techniques, incomplete parameterizations, and inconsistencies between surface and satellite measurements. Schweiger and Key (1994) find errors up to 20 W m^{-2} between different observations of net surface radiation.

Many global climate models do a poor job of representing the seasonal cycle of cloud cover in the Arctic Ocean (Tao et al. 1996). The model used here does successfully capture the seasonal cycle of cloud cover as shown in Fig. 6. Beesley and Moritz (1999) address the interesting question of why the Arctic cloud cover increases in summer. They used a radiative–turbulent column model to investigate three hypotheses: 1) advection from the landmass of air masses of higher specific humidity than over the pack ice, 2) evaporation at the surface of the pack ice, and 3) a temperature-dependent formation and precipitation of atmospheric ice. Their model suggests that the third hypothesis is important in the increase in summertime cloudiness. An observational study by Kukla and Robinson (1988) tends to support the first hypothesis. Our model allows us to comment somewhat on the first two hypotheses. For the control simulation, 44% of the annual precipitation is derived from local evaporation and 56% is derived from atmospheric moisture advection into the Arctic. In July, Table 6 shows that only 28% of the precipitation is derived from local evaporation. This implies that the advective source of water vapor available for cloud formation becomes relatively more important than evaporation during summer. In some local regions this could be reversed.

Another possible reason why the model's clouds increase in summer is related to the model's specific humidity increase in summer. When a perturbation of thermal radiation (e.g., suddenly cooler air above) increases emission from a layer, the lost heat comes from sensible heat or from condensation. When the specific humidity of the layer is greater, more of the heat comes from condensation, which means thicker clouds. This is an important reason why there are more or thicker clouds in July than in January. Both cloud cover and cloud optical depth contribute to the total radiative effects of clouds. For the control, cloud optical depth varies between 3 in winter and 13 in summer. Using observations of Arctic clouds, Kukla and Robinson (1988) found a range of 2–25 for optical depth, and Curry and Ebert

(1992) obtained values between 2 and 8 when weighted by cloud fraction.

Table 2 shows that the net heat from the surface in the control is 10.35 W m^{-2}. The upward sensible and latent heat fluxes are of comparable magnitude (11.5 and 9.8 W m^{-2}) and the energy of precipitation (snow) is 2.7 W m^{-2}. The model's sensible heat flux over the winter ice pack at the latitude of the SHEBA site is downward (1–7 W m^{-2}) and consistent with the SHEBA observations of Guest et al. (2001). The control run is not in balance as indicated by the net energy change (0.44 W m^{-2}) in Table 2. This value indicates a drift in the control simulation of about 0.001°C yr^{-1} and is not a lack of precision of the model's diagnostics. The model's mean annual atmospheric heat transport into the Arctic region (103 W m^{-2}) is also consistent with Nakamura and Oort's 98 W m^{-2} and with the value of 102 W m^{-2} found by Masuda (1990). As shown in Table 2, the model's oceanic heat transport for the present climate is 10.7 W m^{-2} (9.1 ocean liquid transport and 1.6 sea ice transport), which is in good agreement with the observations of Aagaard and Greisman (1975). The model's seasonal cycle of surface air temperature is in good agreement with observations (Fig. 12).

The model's seasonal cycle of sea ice cover indicates that there is too much sea ice in all months in comparison with the Atmospheric Model Intercomparison Project (AMIP) observations (Fig. 7). The sea ice extends southward too far with sea ice cover in the Barents Sea of 86% and 67% for January and July compared with observed values of 36% and 5%. In the central Arctic the model's January sea ice cover (95%) is about the same as the AMIP observations (97%). For the model's 2-m-thick ice in the central Arctic, the model's lead parameterization would ensure at least 3% open water. The model's overall average sea ice thickness for the Arctic is 2.3 m, which is somewhat low. In the central Arctic, there is little change in the model's ice thickness between January and July. The model's sea ice that is too thin could be due to the lack of parallel side stresses that would reduce sea ice advection. The model's excessive horizontal extent of sea ice can be caused by several different features including how the model apportions heat into vertical or lateral melting or freezing of ice. The inclusion of an ice parameterization that includes ice thickness distribution (e.g., Bitz et al. 2001) might improve the model's ice thickness and ice cover. The model's rate of decrease of sea ice cover in the GHG experiment is consistent with the observed rate of decrease in the Arctic Ocean found by AMIP (see Fig. 2 for reference) for the last four decades of the twentieth century. For the GHG experiment, however, Fig. 2, shows a significant increase in sea ice cover after 2000 before the long-term decrease begins again after year 2020.

REFERENCES

Aagaard, K., and P. Greisman, 1975: Toward new mass and heat budgets for the Arctic Ocean. *J. Geophys. Res.,* **80,** 3821–3827.

Andreas, E. L, C. W. Fairall, P. S. Guest, and P. O. G. Persson, 1999: An overview of the SHEBA atmospheric surface flux program. Preprints, *Fifth Conf. on Polar Meteorology and Oceanography,* Dallas, TX, Amer. Meteor. Soc., 411–416.

Barkstrom, B. R., E. F. Harrison, and G. L. Smith, 1989: Results from the Earth Radiation Budget Experiment (ERBE). *Adv. Space Res.,* **9,** 775–782.

Beesley, J. A., 2000: Estimating the effect of clouds on the arctic surface energy budget. *J. Geophys. Res.,* **105,** 10 103–10 117.

——, and R. E. Moritz, 1999: Toward an explanation of the annual cycle of cloudiness over the Arctic Ocean. *J. Climate,* **12,** 395–415.

Bitz, C. M., M. M. Holland, A. J. Weaver, and M. Eby, 2001: Simulating the ice-thickness distribution in a coupled climate model. *J. Geophys. Res.,* **106,** 2441–2463.

Chiacchio, M., J. Francis, and P. Stackhouse, 2002: Evaluation of methods to estimate the surface downwelling longwave flux during Arctic winter. *J. Appl. Meteor.,* **41,** 306–318.

Curry, J. A., and E. E. Ebert, 1992: Annual cycle of radiation fluxes over the Arctic Ocean: Sensitivity to cloud optical properties. *J. Climate,* **5,** 1267–1280.

——, and Coauthors, 2000: FIRE Arctic Clouds Experiment. *Bull. Amer. Meteor. Soc.,* **81,** 5–29.

Deser, C., J. E. Walsh, and M. S. Timlin, 2000: Arctic sea ice variability in the context of recent atmospheric circulation trends. *J. Climate,* **13,** 617–633.

Fletcher, J. O., 1965: The heat budget of the Arctic Basin and its relation to climate. The Rand Corporation Rep. R-444-PR, 175 pp.

Gates, W. L., and Coauthors, 1999: An overview of the results of the Atmospheric Model Intercomparison Project (AMIP). *Bull. Amer. Meteor. Soc.,* **80,** 29–55.

Guest, P. S., P. O. G. Persson, E. L Andreas, and C. W. Fairall, 2001: What is the role of the sensible heat flux on the surface heat budget of multi-year sea ice? Preprints, *Sixth Conf. on Polar Meteorology and Oceanography,* San Diego, CA, Amer. Meteor. Soc., J9–J12.

Houghton, J. T., L. G. Meira Filho, B. A. Callander, N. Harris, A. Kattenberg, and K. Maskell, Eds.,1996: *Climate Change 1995: The Science of Climate Change.* Cambridge University Press, 572 pp.

Huschke, R., 1969: Arctic cloud statistics from ''air-calibrated'' surface weather observations. The Rand Corporation Rep. RM-6173-PR, 79 pp.

Key, J., R. S. Silcox, and R. S. Stone, 1996: Evaluation of surface radiative flux parameterizations for use in sea ice models. *J. Geophys. Res.,* **101,** 3839–3849.

Kukla, G. J., and D. A. Robinson, 1988: Variability of summer cloudiness in the Arctic Basin. *Meteor. Atmos. Phys.,* **39,** 42–50.

Large, W. G., J. C. McWilliams, and S. C. Doney, 1994: Oceanic vertical mixing: Review and a model with non-local boundary layer parameterization. *Rev. Geophys.,* **32,** 363–403.

Lucarini, V., and G. L. Russell, 2002: Comparison of mean climate trends in the Northern Hemisphere between NCEP and two atmosphere–ocean model forced runs. *J. Geophys. Res.,* in press.

Masuda, K., 1990: Atmospheric heat and water budgets of polar regions: Analysis of FGGE data. *Proc. NIPR Symp. on Polar Meteorology and Glaciology,* Tokyo, Japan, National Institute of Polar Research, 79–88.

Miller, J. R., and G. L. Russell, 1997: Investigating the interactions among river flow, salinity and sea ice using a global coupled atmosphere–ocean–ice model. *Ann. Glaciol.,* **25,** 121–126.

——, and ——, 2000: Projected impact of climate change on the freshwater and salt budgets of the Arctic Ocean by a global climate model. *Geophys. Res. Lett.,* **27,** 1183–1186.

——, ——, and G. Caliri, 1994: Continental scale river flow in climate models. *J. Climate,* **7,** 914–928.

Nakamura, N., and A. H. Oort, 1988: Atmospheric heat budgets of the polar regions. *J. Geophys. Res.,* **93,** 9510–9524.

Perovich, D. K., and Coauthors, 1999: Year on ice gives climate insights. *Eos, Trans. Amer. Geophys. Union,* **80,** 481, 485–486.

Randall, D., and Coauthors, 1998: Status of and outlook for large-scale modeling of atmosphere–ice–ocean interactions in the Arctic. *Bull. Amer. Meteor. Soc.,* **79,** 197–219.

Rind, D., R. Healy, C. Parkinson, and D. Martinson, 1995: The role of sea ice in $2 \times CO_2$ climate model sensitivity. Part I: The total influence of sea-ice thickness and extent. *J. Climate,* **8,** 449–463.

——, ——, ——, and ——, 1997: The role of sea ice in $2 \times CO_2$ climate model sensitivity: Part II: Hemispheric dependencies. *Geophys. Res. Lett.,* **24,** 1491–1494.

Rinke, A., A. H. Lynch, and K. Dethloff, 2000: Intercomparison of Arctic regional climate simulations: Case studies of January and June 1990. *J. Geophys. Res.,* **105,** 29 669–29 683.

Russell, G. L., J. R. Miller, and D. Rind, 1995: A coupled atmosphere–ocean model for transient climate change studies. *Atmos.–Ocean,* **33,** 683–730.

——, ——, ——, R. A. Ruedy, G. A. Schmidt, and S. Sheth, 2000: Comparison of model and observed regional temperature changes during the past 40 years. *J. Geophys. Res.,* **105,** 14 891–14 898.

Schweiger, A. J., and J. R. Key, 1994: Arctic Ocean radiation fluxes and cloud forcing based on the ISCCP-C2 cloud dataset. *J. Appl. Meteor.,* **33,** 948–963.

Serreze, M. C., and Coauthors, 2000: Observational evidence of recent change in the northern high-latitude environment. *Climate Change,* **46,** 159–207.

Shea, D., 1986: Climatological atlas, 1950–1979: Surface air temperature, precipitation, sea-level pressure and sea-surface temperature (45°S–90°N). NCAR Tech. Note 269+STR, National Center for Atmospheric Research, Boulder, CO, 35 pp.

Tao, X., J. E. Walsh, and W. L. Chapman, 1996: An assessment of global climate simulations of Arctic air temperatures. *J. Climate,* **9,** 1060–1076.

Uttal, T., and Coauthors, 2002: Surface heat budget of the Arctic Ocean. *Bull. Amer. Meteor. Soc.,* **83,** 255–275.

Weatherly, J. W., and Y. Zhang, 2001: The response of the polar regions to increased CO_2 in a global climate model with elastic–viscous–plastic sea ice. *J. Climate,* **14,** 268–283.